

Modeling and optimization of thermal conductivity of stabilized γ -Al₂O₃ /water nanofluid using response surface methodology (RSM)

Abstract

The present study estimates thermal conductivity ratio (KR) of stabilized γ -Al₂O₃ /water nanofluid by response surface methodology (RSM). This study was operated under experimental conditions with solid volume fractions of SVF=0.05–2%, and temperature of T=25–45 °C. Sedimentation visualization and dynamic light scattering (DLS) were performed to test the stability of nanofluids. The results of monitoring the stability of nanofluid with sedimentation visualization method showed that it was stable for at least 24 h. Different models were evaluated based on a series of quality indicators and charts. Some of the indicators that were investigated in this study include standard deviation (Std. Dev.), coefficient of determination (R²) and coefficient of variation (C.V). After checking the quality indicators and charts for different models, the quadratic model was selected as the optimal model. The values of Std. Dev, R² and C. V for the quadratic model were 0.0241, 0.9785, and 1.87, respectively. Also, adjusted R² and predicted R² parameters of the quadratic model were equal to 0.9606 and 0.8776 respectively, which signifies the accuracy of the model. The residual plot, the normal probability plot, the Box-Cox plot and the predicted vs. actual plot also showed that quadratic model has a good accuracy, and is well capable of estimating the KR of the nanofluid. The most optimum KR is 1.485. At a temperature of 45 °C, this condition was achieved in samples at SVF=1.764%.

Keywords: Stability, DLS, Sedimentation, Standard deviation, Optimum

1. Introduction

In many engineering applications, base fluids like water, oils, and glycols are utilized as operational fluids in heat exchange systems. Improving the base fluids' thermal conductivity can raise the devices' thermal efficiency. The idea that solid particles the size of nanometers can disperse in base fluids was evolved by Choi et al. [1] has grown to be a significant subject known as nanofluids. In order to be able to research about nanofluids, preparing these types of fluids in a stable form is a very important factor, because the stability of nanofluids strongly affects its thermophysical properties [2, 3]. The type, size, shape, concentration, base fluid, operating temperature, and addition of surfactant all affect the thermophysical properties of dispersed nanoparticles in nanofluids [4-6]. In addition, although augmenting the nanoparticle concentration enriches the thermophysical features of the nanofluid, there is a penalty for changing the stability behavior [7-9]. Hence, optimizing parameters poses a significant challenge for researchers [10]. Thermal conductivity is a crucial physical feature of nanofluids that warrants further investigation. As a result, numerous researchers have accomplished various experimental and numerical studies to determine the thermophysical features of nanofluids [11-20]. It is crucial to research the factors that have an important effect on these features. Numerous researchers have looked into the thermophysical features of varied nanoparticles in current years in various base fluids [21-28]. Esfe et al. [29] accomplished a laboratory examination into the thermal conductivity of nanofluids suspended in water, including 5 nm-diameter Al_2O_3 nanoparticles. The thermal conductivity of Al_2O_3 /water was measured within a temperature range of 26 to 55 °C. The findings demonstrated that raising the temperature at any concentration significantly grown the thermal conductivity of nanofluids. Putra et al. [30] the thermal conductivity of Al_2O_3 /water nanofluid with an average nanoparticle size of 131 nm was experimentally studied. The findings proven that the nanofluid's thermal conductivity rose by approximately 24% when the concentration was increased to 4%. Zhang et al. [31] have performed an experimental study to find how the concentration of Al_2O_3 /water nanofluid affected the thermal conductivity. The thermal conductivity increased by 15% when the concentration was increased to 5%. Masuda et al. [32] researched the thermal conductivity of titanium oxide and aluminum oxide in water-based fluid through experimentation and demonstrated that these nanofluids' thermal conductivity increases by 10% and 30%, respectively, when compared to water at a concentration of 4%. Eastman et al. [33] observed a 40% rise in CuO-EG nanofluid thermal conductivity at 0.3 vol%. Murshed et al. [34] investigated the thermal conductivity of water-based titanium oxide nanofluid that had rod and spherical forms. Their findings demonstrated that a significant factor in raising the thermal conductivity of the nanofluid is the shape of the particles. After comparing the experimental outcomes with theoretical models, it was discovered that the thermal conductivity values of nanofluids obtained from experiments were higher than those estimated by the models. Mintsa et al. [35] have documented that concentration and

temperature impact the enhance in thermal conductivity in nanofluids of copper oxide (47 nm) and aluminum oxide (36 nm). A study carried out by Abdel-Samad et al. [36] have demonstrated that as temperature and concentration rise, the thermal conductivity of the titanium oxide-water nanofluid accelerates. They found that at 90°C, there was an increase in thermal conductivity of 37.35% with a volume fraction of 0.47%, whereas at 20°C, there was an increase of 24.11%. Eshgarf et al.[37] investigated the viscosity and thermal conductivity of an iron oxide-water nanofluid at various temperatures and concentrations. Next, artificial neural networks (ANNs) were utilized to progress models for forecasting the thermophysical properties mentioned. According to these findings, the suggested models could forecast the thermophysical characteristics of nanofluids with great accuracy. The statistical modeling method known as response surface methodology (RSM) describes the interconnectivity of system inputs and outputs using mathematical models [38]. The ability of RSM to capture the non-linear relationships between the inputs and the outputs has demonstrated its effectiveness in modeling the thermophysical characteristics of nanofluids [39, 40]. Peng et al. [41] have presented the findings of a trustworthy model utilizing RSM to predict the thermal conductivity of CuO/water nanofluid at varied temperatures and concentrations. Esfe et al.[42] examined the rheological behavior of the HNF (Hybrid Nanofluid) containing MWCNT-SiO₂ (10:90) with the RSM. The main objective of this study was to introduce a new correlation. Khetib et al. [43] used RSM to investigate the viscosity of a paraffin-based CuO nanofluid. Experiments conducted at T = 25–100 °C and mass fractions of 0 –25% provided the data used in the modeling. RSM shows that compared to second degree and linear polynomials, the results obtained from the third degree polynomial are more accurate. Table 1 shows an overview of prior researches on the use of RSM in estimating the thermal conductivity of nanofluids.

Table 1. Applications RSM in forecasting thermal conductivity of nanofluid.

References	Nanoparticles	Base fluid	Remarks
Peng et al.[41]	CuO (II)	Water	R ² = 0.9939 AAD% = 0.615%
Esfe et al.[44]	Al ₂ O ₃	EG/water	R ² = 0.9982,
Esfe & Hajmohammad [22]	ND+Co ₃ O ₄	EG/water	R ² = 0.9957 Std. Dev = 0.002516
Khetib et al. [45]	ND + Fe ₃ O ₄	EG/water	R ² =0.994 MSE=2.0297×10 ⁻⁶
Khetib et al.[46]	Fe ₃ O ₄	Water	R ² =0.998 MSE=0.0013
Malika & Sonawane [39]	Fe ₂ O ₃ + SiC	Water	R ² = 0.969 AAD% = 1.165%
Shahsavari et al.[47]	GO+Fe ₃ O ₄ +TiO ₂	oil	R ² =0.9898 Adjusted R ² =0.9895 Predicted R ² =0.9888 Std. Dev =0.1856 C.V% =1.31%

Borode & Olubambi[48]	GNP+ Al ₂ O ₃	Water	R ² =0.9882 Adjusted R ² =0.9840 Predicted R ² =0.9721 Std. Dev =0.0020 C.V% =0.3263%
Esfe et al.[49]	MWCNT+ Al ₂ O ₃ + ZnO	Water	R ² =0.9972 Adjusted R ² =0.9968 Predicted R ² =0.9962 Std. Dev =4.447 ×10 ⁻³ C.V% =0.4% -1.05% <MOD <+ 1.08%
Esfe et al.[50]	MWCNT+TiO ₂	EG/water	R ² = 0.9957 Adjusted R ² =0.9934 Predicted R ² =0.9909 Std. Dev =0.0082 C.V% =0.6799% -1.754% <CD% <+ 0.9615%

AAD: average absolute deviation
 C.D: correlation deviation
 C.V: coefficient of variation
 Std. Dev: standard deviation
 R²: coefficient of determination
 MOD: margin of deviation
 MSE: mean square error
 GNP: graphene nanoplatelets
 ND: Nanodiamond

The first part of this study deals with the preparation of Al₂O₃/water nanofluid, stabilization method and stability measurements. Then the method of measuring thermal conductivity is defined. The reasons for choosing Al₂O₃ nanoparticle are its desirable features such as reasonable price, the possibility of various applications, availability with high purity, high thermal and corrosion resistance, strength and high degree of mechanical hardness, and favorable environmental compatibility. Then, the design of the experiment, the formation of the model and the accuracy of the model with respect to the experimental data are investigated using Design Expert software (13.0.0). We establish a correlation that is dependent on the interaction of operating parameters and evaluate its reliability with experimental data. Based on the literature, it can be realized that most of the models developed for the prediction of thermal conductivity have certain limitations that limit the application of the correlations to other nanofluids. So, the primary objective of this work is to evaluate the possible effect of the operating temperature and also the SVF (solid volume fraction) and their interactions on the thermal conductivity of the nanofluid. The other goal of this study is the optimization of parameters to maximize thermal conductivity of the system using RSM. The last goal of this research was to compare the outcomes of the estimation of RSM model with other models presented in the literature.

2. Nanofluid preparation and property measurement

2.1 Nanofluid preparation and stability check

There are two methods for nanofluid production, including one-step and two-step. Due to the commercial availability of nanoparticles, numerous researchers have developed a two-part process for manufacturing nanofluid. Specification of γ -alumina nanoparticles (obtained from US Research Nanomaterials, Inc.) is displayed in Table 2. Transmission electron microscopy (TEM) was employed to estimate the size of primary nanoparticles. Based on the illustration in Fig.1, it is evident that the nanoparticles have an approximately spherical shape.

Table 2. Specification of nanoparticle used in this study.

Nanoparticle	Aluminum Oxide (γ)
Average particle size (nm)	20
Purity	>99%
Density (kg/m^3)	3890
Color	White
Morphology	Nearly spherical
Specific area (m^2/g)	>138
Specific heat (J /kg K)	880
Thermal conductivity(W/m K)	46

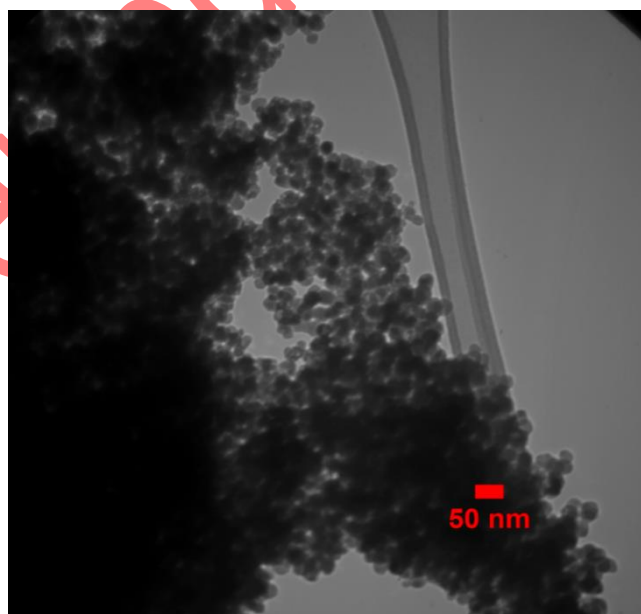


Fig.1. Image of TEM nanoparticles used in this study.

In this study, a two-step method was used to prepare nanofluids. The stability of nanofluids is a significant concern in this technique. Both thermophysical and heat transfer properties are closely

tied to stability of a nanofluid [51]. The long-term stability of nanofluids is a crucial factor in determining their practical applicability. In this study, the concentration (0.05, 0.5, 1, and 2 vol%) and temperature (25, 35, and 45 °C) of the nanofluids were chosen. Alumina nanoparticles are added to distilled water as the base fluid, and their weight is measured to four decimal places. The fluid was stirred with a magnetic stirrer for one hour and then transferred to an ultrasonic vibrator (BANDELIN Company - power 240 W and frequency 35 kHz) for three hours. In this study, we employed sedimentation visualization and dynamic light scattering (DLS) to assess the stability of nanofluids. The results of monitoring the stability of nanofluid with sedimentation visualization method showed that it was stable for at least 24 h. The mentioned method is used in references [52-56]. The size distribution of nanoparticles in the dispersed phase is detected by DLS. DLS technique was employed to obtain the distribution of particle size in nanofluids using a Malvern Zetasizer Nano (Malvern Panalytical, UK) for studying clustering and agglomeration phenomena. Samples, both fresh and old (after 7 days), were analyzed to determine the particle size distribution. The findings are outlined in Table 3. Because DLS measures the hydrodynamic radius of nanoparticles, the average size obtained by these particles was larger than what could be seen through a micrograph of TEM. The findings also indicate that a raise in the vol. fraction of nanofluid leads to a larger particle size. The increased agglomeration of nanoparticles upon their addition to the basefluid can be attributed to this phenomenon. In addition, the results show that freshly prepared nanofluids in different concentrations have larger average diameter of nanoparticles than nanofluids after 7 days old. Such a phenomenon is related to the fact that the larger aggregated particles settle, and this causes the easy detection of smaller particles by DLS [57, 58]. The mentioned findings are in agreement with the results of studies [57, 59, 60].

Table 3. Average diameter of nanoparticles at different times obtained from dynamic light scattering (DLS).

Concentration (vol.%)	Nanoparticle diameter (nm)	
	freshly	7 days old
0.05	134	90
0.5	161	129
1	169	147
2	218	197

2.2 Measurement of thermal conductivity

A KD2 Pro thermal properties analyzer (Decagon Devices, Inc. USA, Fig 2) was applied to measure the thermal conductivity of the nanofluid under different experimental conditions. The measurement works in the range of 0.02-2 W/m.K. This device is fitted with a KS-1 type needle sensor, which is placed vertically and centrally in the nanofluid container. The temperature of the sample was controlled with the aid of a water bath during the measurement process. To avoid the possibility of transient heat effects, a 30-minute interval between subsequent measurements was chosen to

minimize their effect on the temperature increase near the probe. Therefore, the obtained results are stable and repeatable. To achieve precision and consistent results, the average of three thermal conductivity measurements for each sample is used. The uncertainties in thermal conductivity measurements was predicted based on the accuracies of the tools given in table 4 and calculated by the method [61].The maximum uncertainty in the measured thermal conductivity was 1.8 %.

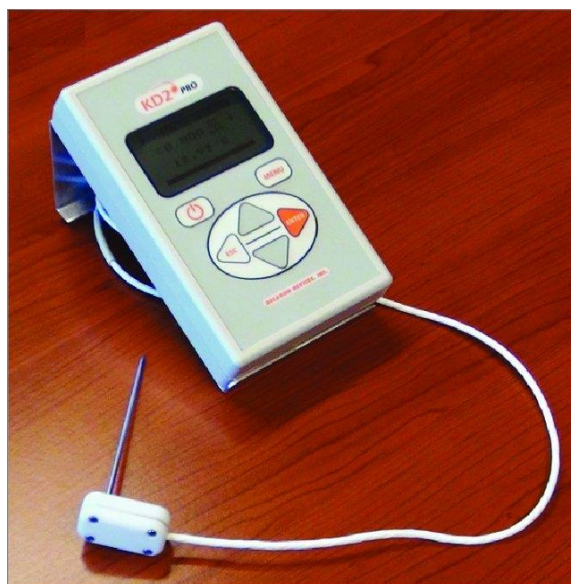


Fig. 2. Thermal properties analyzer device

Table 4. Accuracy of the instruments.

Instruments	Accuracy
Weighing balance	± 0.0001
Ultrasonic bath	± 3 kHz
Thermal conductivity apparatus	± 0.01 W/m.K
Water bath	± 0.1 °C

3.RSM

Many engineering phenomena have been modeled using theories. A suitable mathematical model for many phenomena is not available due to various controlling factors, computational complexity, or unknown mechanisms. Experimental modeling techniques are efficient. One of the approaches to experimental modeling is RSM. In this approach, the response variable is affected by numerous independent input parameters, aiming to optimize the response variable and analyze the factors impacting it while minimizing the number of tests conducted. Response surface methodology (RSM) has many applications in different topics such as essential oil [62] and seed oil extraction [63, 64], optimization and mathematical modeling [65, 66], impregnation [67, 68], nanoparticle formation [69-71], and etc.

4. Results and discussion

The purpose of the RSM evaluation is to apply a statistical regression approach to model the correlation between the input variable SVF and T and the output response variable ($KR = \text{thermal conductivity ratio} = \frac{K_{nf}}{K_{bf}}$) of the nanofluid. Table 5 displays the p-values, Adjusted R^2 and Predicted R^2 values for the linear, two-factor interaction (2FI), quadratic and cubic models that were examined in the analysis.

Table 5. Summary of statistics for the various models.

Source	Sequential p-value	Adjusted R^2	Predicted R^2	
Linear	0.0002	0.8156	0.7353	
2FI	0.7769	0.7948	0.6797	
Quadratic	0.0030	0.9606	0.8776	Suggested
Cubic	0.2971	0.9534	0.8113	Aliased

The sequential p-value column denotes the importance level of each model term as they were sequentially added to the model. It quantifies the probability of achieving the recorded data or even more extreme results under the assumption that the null hypothesis holds true. A p-value below 0.05 indicates that the term is statistically important, signifying its impact on the variability of the response variable [72]. The Adjusted R^2 value indicates the proportion of the overall variance in the dependent variable that is determined by the model, while also considering the quantity of independent variables included. A higher Adjusted R^2 value implies a better fit between the model and the data. The Predicted R^2 column displays the anticipated proportion of variability in forthcoming observations that the model can clarify. A greater Predicted R^2 value suggests that the model is expected to demonstrate strong performance when applied to new data. From this table, we can see that the quadratic model has the best Adjusted R^2 (0.9606) and Predicted R^2 (0.8776), which shows that it is the most accurate model to provide the best fit to the data and to estimate the response variable. The adjusted R^2 value for the cubic model is also high (0.9534), whereas the adjusted R^2 values for the 2FI and Linear models are comparatively lower. The Cubic model exhibits a low Predicted R^2 (0.8113) and is marked as Aliased, indicating that it cannot be differentiated from another model due to collinearity or confounding factors. Hence, the quadratic model has been chosen for further examination in this study. Table 6 displays the results of the ANOVA analysis for the quadratic model. The sources of variability are presented, along with their corresponding sum of squares, degrees of freedom, mean square, F-value, and p-value. The F-value is utilized in ANOVA to assess the statistical importance of the variation among factors [73]. The model is considered statistically significant with an F-value of 54.59, indicating that the probability of obtaining such a high F-value by random chance is extremely low at 0.01%. The results indicate that both factors the SVF (A) and

temperature (B) have extremely low p-values (<0.0003), signifying their significant influence on the response. Both the AB interaction term and B^2 have p-values that exceed 0.05, suggesting that they are not statistically important. Conversely, A^2 possesses a p-value of 0.0012, denoting its significance as a term.

Table 6. ANOVA outcome for the suggested quadratic model.

Source	Sum of Squares	df	Mean Square	F-value	p-value	
Model	0.1581	5	0.0316	54.59	< 0.0001	significant
A-SVF	0.1134	1	0.1134	195.68	< 0.0001	
B-T	0.0337	1	0.0337	58.19	0.0003	
AB	0.0003	1	0.0003	0.4471	0.5286	
A^2	0.0193	1	0.0193	33.30	0.0012	
B^2	0.0014	1	0.0014	2.33	0.1778	
Residual	0.0035	6	0.0006			
Cor Total	0.1616	11				

Table 7 shows the fit statistics of the quadratic model. The table denotes that the Predicted R^2 value of 0.8776 nearly matches the Adjusted R^2 value of 0.9606, with a difference of less than 0.2. This indicates that the model can be trusted when making estimations for future observations. The Adeq Precision assesses the model's quality by comparing the variation present in the data with the variation anticipated by the model. A ratio exceeding 4 is deemed satisfactory, and a viewed ratio of 23.2535 suggests that the model is suitable for exploring the design space.

Table 7. Fit statistics for the quadratic model.

Std. Dev.	Mean	CV %	R^2	Adjusted R^2	Predicted R^2	Adeq Precision
0.0241	1.29	1.87	0.9785	0.9606	0.8776	23.2535

Table 8 exhibits the coefficient estimates, degrees of freedom, standard error, 95% confidence interval, and Variance Inflation Factors (VIFs) for each factor in the KR. The coefficient estimate signifies the anticipated alteration in the response when the value of a factor changes by one unit, while all other factors remain constant. In an orthogonal design, the intercept represents the mean response of all the runs. The coefficients indicate adjustments to the mean response according to the factor configurations. When the factors are orthogonal, the Variance Inflation Factors (VIFs) will be equal to 1. VIFs exceeding 1 indicate the existence of multicollinearity, with a stronger correlation between factors as the VIF value increases. Typically, VIFs that are below 10 are considered acceptable. The intercept coefficient estimate is 1.34, which suggests the average response of all runs when all variables are set to their baseline values. The coefficient estimate for factor A (SVF) is 0.1318, indicating that a one-unit increase in SVF leads to a 0.1318 increase in the response, while all other factors remain constant. The factor B (temperature) has a coefficient estimate of 0.0661, suggesting that a one-unit increase in temperature leads to a response increase of 0.0661, while

holding all other factors constant. The AB coefficient estimate is 0.0077, denoting that the interaction between factors A and B has a very minor positive effect on the response. The coefficient estimate for A^2 is -0.0920, indicating that a one-unit increase in A^2 leads to a reduction of 0.0920 in the response, while all other factors held constant. The coefficient estimate for B^2 is 0.0225. Additionally, VIFs offer insights into the collinearity present among factors. In this instance, they are all near or below 1.04, indicating that collinearity is not a significant concern in the model.

Table 8. Coefficient estimate in terms of the coded factors.

Factor	Coefficient Estimate	df	Standard Error	95% CI Low	95% CI High	VIF
Intercept	1.34	1	0.0153	1.31	1.38	
A-SVF	0.1318	1	0.0094	0.1088	0.1549	1.02
B-T	0.0661	1	0.0087	0.0449	0.0873	1.04
AB	0.0077	1	0.0114	-0.0204	0.0357	1.04
A^2	-0.0920	1	0.0159	-0.1310	-0.0530	1.02
B^2	0.0225	1	0.0147	-0.0136	0.0586	1.0000

The relationship between the KR and the actual values of the SVF and T factors is illustrated in Eq. (1). The coefficients assigned to each factor determine their individual impact on KR, while the interaction term signifies the combined effect of both factors. This equation, different the coded one, is meant to forecast the actual response values in their original units. Nevertheless, it is not possible to compare the coefficients in order to assess the relative strength of each factor, as they have been adjusted to match with the units of each factor. Furthermore, the center of the design space is not depicted by the intercept.

$$KR = 1.17601 + 0.306159 * SVF - 0.009947 * T + 0.000785 * SVF * T - 0.096795 * SVF^2 + 0.000225 * T^2 \quad (1)$$

The perturbation plot in Fig. 3 demonstrates the effect of two factors on the KR response. The diagram visually depicts the relationship between the factors being examined and the system's response. The diagram is created by perturbing a single factor at a time while keeping the other factors fixed and monitoring the resulting alterations in the response. This permits you to visualize the curvature of the response surface and identify interactions between factors. The slope of each line demonstrates the sensitivity of the response to that particular factor, whereas the curvature of the line signifies the existence of any interactions with the other factors. According to Fig. 3, it can be viewed that factor A exerts the greatest influence on the KR, whereas factor B demonstrates the least impact.

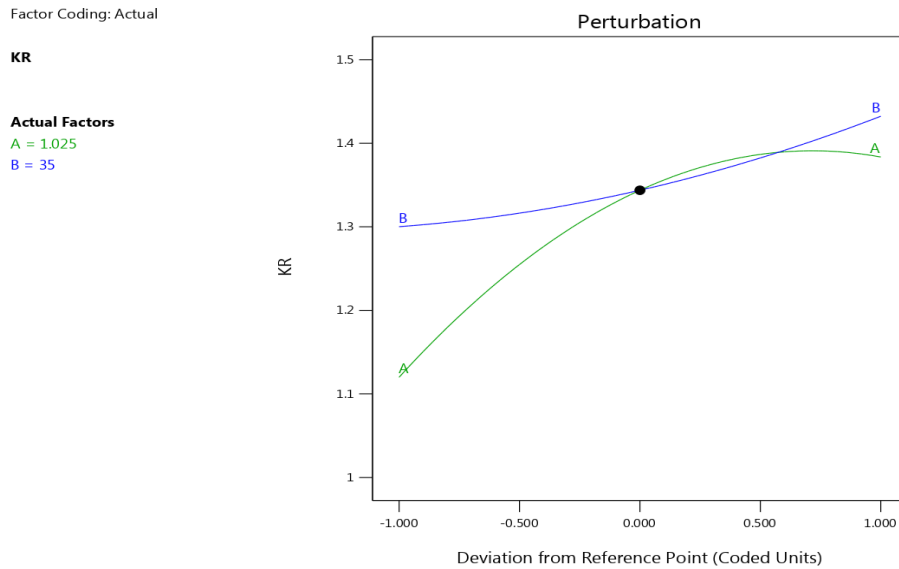



Fig. 3. Perturbation plot of the influence of input factors on the KR.

Fig. 4 displays the comparison of the outcomes gained from the experimental examination with the anticipated results deduced from the correlations suggested by RSM. Fig. 4 demonstrates that the actual and predicted outcomes are nearly similar, with just a few small deviations, as evidenced by Fig. 5(a-c). The studentised residuals distribution is depicted in Fig. 5a, showing that most of the residuals are concentrated near the '0' reference line. This implies that the correlations established are reliable and the models accurately captured the behavior of the data. Furthermore, in Fig. 5b, one can observe a reasonably random distribution of residuals throughout the run order, suggesting that the model adequately addresses the temporal dimension of the data. In Fig. 5c shows the normal probability graph of selected model. This graph illustrates the normal distribution of the residuals and their linearity. Even for typical data, some degree of scattering can be expected. If the data follows an s-shaped curve, it is necessary to employ transfer functions. As shown in Fig. 5c, the selected model is mostly linear with minimal deviation. A normal probability plots is used to evaluate how a small data set is normally distributed.

KR
 Color points by value of
 KR:
 1.09  1.49

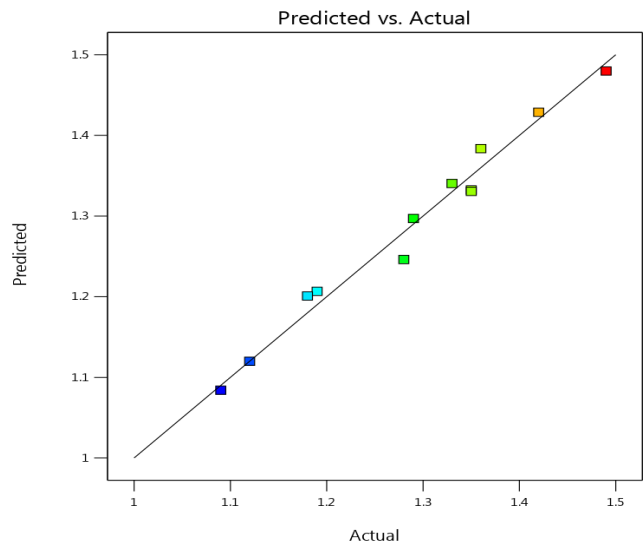
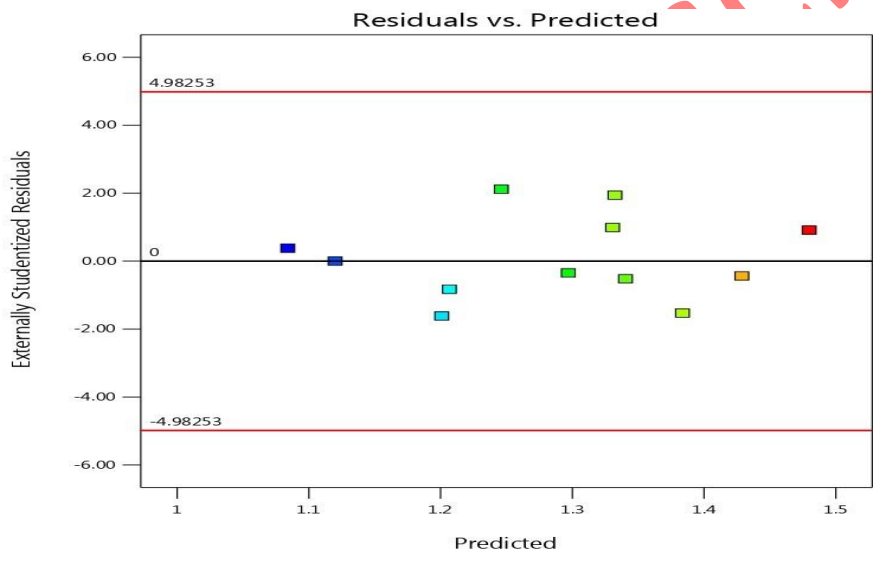
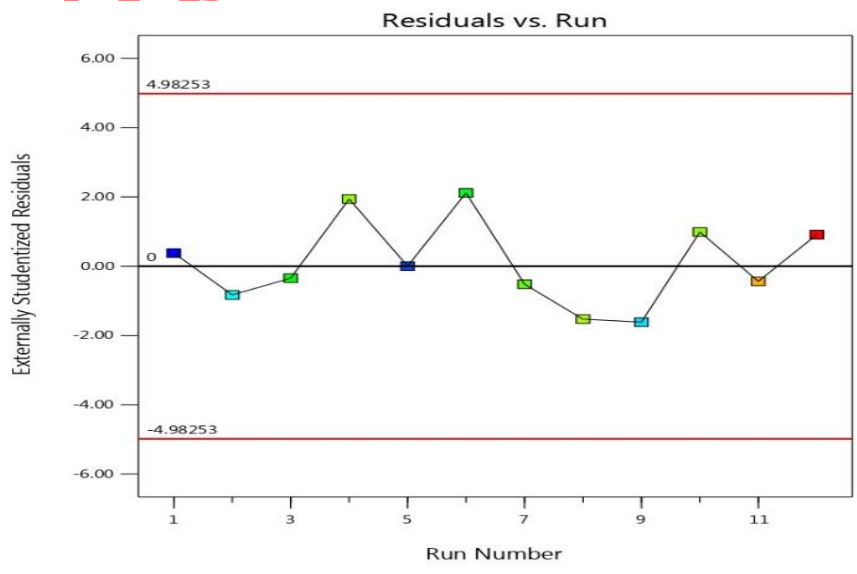


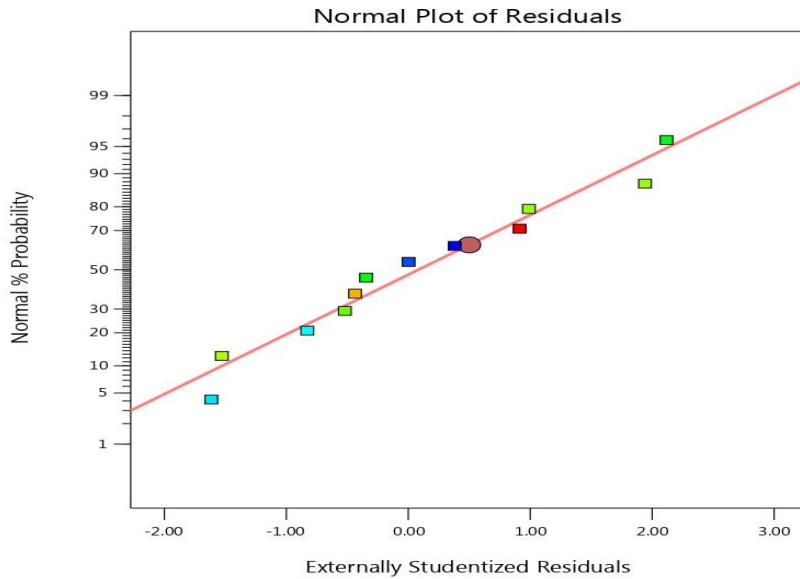
Fig. 4. Correlation between the experimental and predicted values.



(a)



(b)



(c)

Fig. 5. Plot of externally studentised residuals in relation to (a) predicted value (b) run order (c) normal plot

A lambda value of 1 in Box-Cox plot analysis indicates that the original data fits well. Box-Cox plots are utilized to transform the data distribution into a normal distribution. Fig. 6 displays the Box-Cox plots of the quadratic model. This plot offers guidance on selecting the appropriate transfer function. The optimal transfer function is recommended by considering the best lambda value, situated at the minimum point of the curve. If the 95% confidence interval surrounding this lambda includes 1, the software will not suggest any type of transformation. The quadratic model plot, as depicted in Fig. 6, exhibits suitable behavior, with the lambda line predominantly positioned at the lower bottom of the curve.

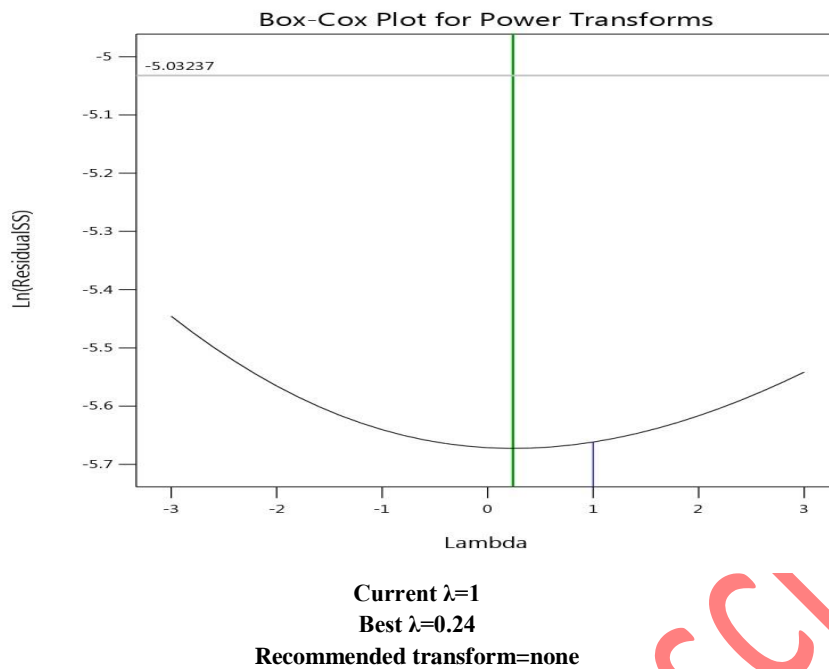


Fig. 6. Box-Cox diagrams for determining Lambda value.

The 2D contour and 3D surface plots in Figs. 7 and 8 demonstrate how different input parameters affect the KR of the nanofluid. Fig. 7 presents a 2D contour illustrating the effect of SVF and T on KR, which helps us understand the relationship between them. Instead, Fig. 8 improves deducing by exhibiting a three-dimensional surface plot that allows a more detailed visualization of the complex interaction between SVF, T and KR. The plot contour lines link points sharing the same KR value, enabling us to pinpoint regions with higher or lower KR values and detect any trends or patterns. Figures indicate that the KR of the nanofluid enhances rapidly as the SVF level rises. Additionally, the figures exhibit that the KR enhances as the temperature raises, (although this effect is not tangible compared to the SVF.), which can be attributed to the increase in Brownian motion due to increasing temperatures. These results align with earlier research studies that have been published [74, 75].

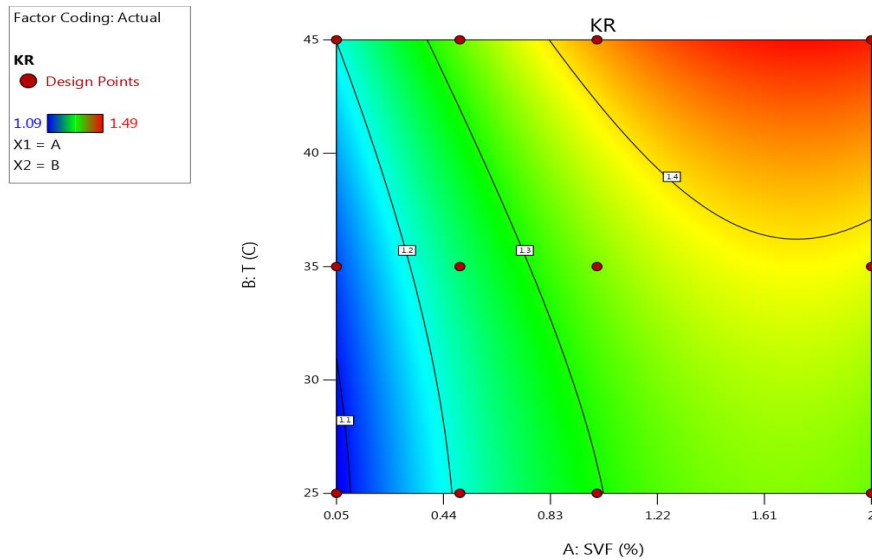


Fig. 7. 2D contour plot of the impact of SVF and T on the KR.

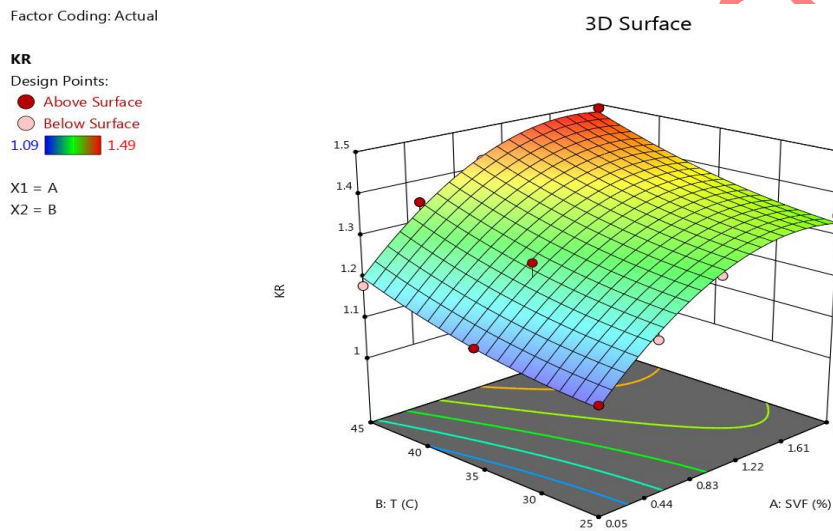


Fig. 8. 3D surface plot of the impact of SVF and T on the KR.

5. Optimum response

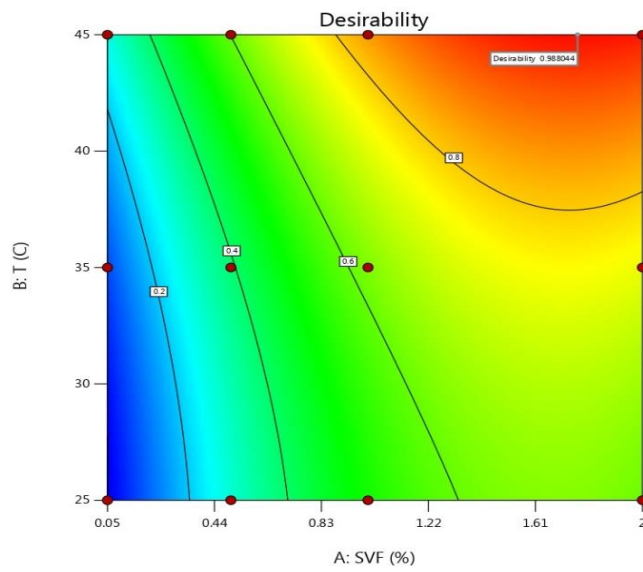
An optimization was performed on the thermal conductivity ratio (KR) of the Al_2O_3 /water nanofluid to achieve its maximum value. This optimization involved adjusting the SVF and T of the nanofluid. In order to optimize the process, the KR of the nanofluid was maximized by utilizing the correlation acquired through RSM. The optimization results demonstrated that the nanofluid's KR is maximized at 45 °C, reaching 1.485, within the investigated range of T (25 to 45 °C) and SVF (0.05 to 2% vol.). Achieving this value is possible only when the SVF of the nanofluid is adjusted to 1.764%. Table 9 showcases a range of optimal solutions for nanofluid. Fig. 9(a&b) displays the value of desirability and optimal values of KR at different points.

Table 9. Different optimal solutions for nanofluid.

Number	SVF	T	KR	Desirability	
1	1.764	45.000	1.485	0.988	Selected
2	1.754	45.000	1.485	0.988	
3	1.780	45.000	1.485	0.988	
4	1.744	45.000	1.485	0.988	
5	1.808	45.000	1.485	0.988	
6	1.879	45.000	1.484	0.985	
7	1.598	45.000	1.483	0.981	
8	1.578	45.000	1.482	0.980	
9	2.000	44.046	1.469	0.947	

Factor Coding: Actual

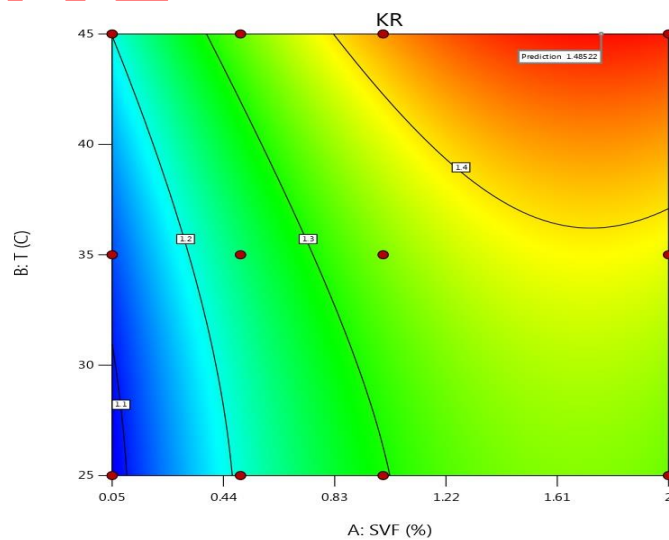
Desirability
 ● Design Points
 0 1
 X1 = A
 X2 = B



(a)

Factor Coding: Actual

KR
 ● Design Points
 1.09 1.49
 X1 = A
 X2 = B



(b)

Fig. 9. Optimal values of KR in different SVF (a) desirability (b) KR.

Fig. 10 shows the comparison of the proposed RSM model with other theoretical and experimental models in the literature, in order to estimate the KR of the nanofluid. As it is clear from the Fig 10,

other models performed poorly in estimation, while the RSM model has a very good match with the experimental data. Also, in table 10, the comparison of different models has been done quantitatively and with different statistical parameters. It is clear in the table that in all statistical parameters, the best results are related to the RSM model. The mentioned findings are in agreement with the results [76]. Table 11 displays the mathematical representation of statistical parameters employed in this research.

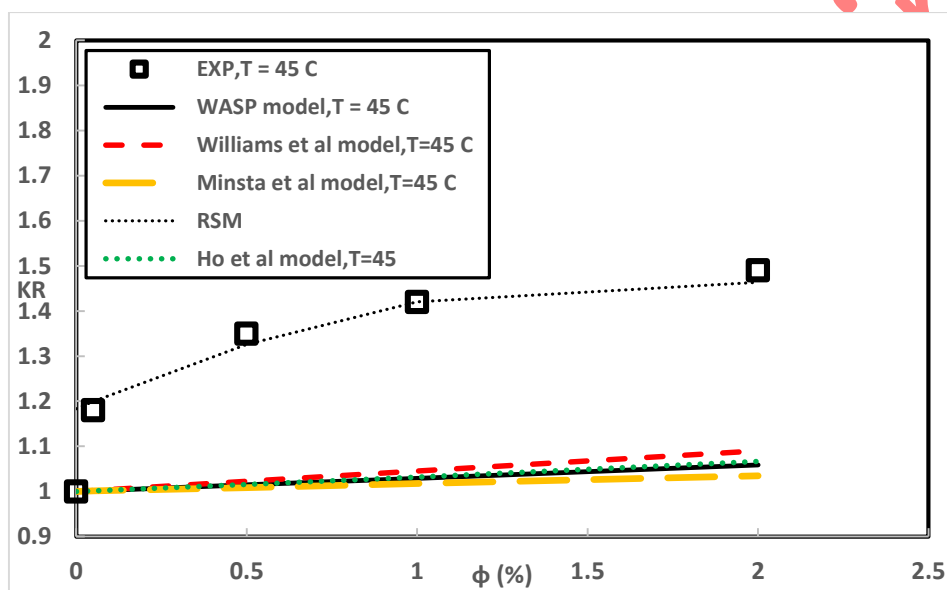


Fig.10. Comparison of different models in forecasting of KR nanofluid.

Table 10. The comparison between the results of the RSM model and other models for estimation of KR nanofluid.

Models	AARD%	MSE	RMSE	Maximum MOD%
WASP [77]	19.3	0.097	0.311	29.2
Williams et al [78]	18.5	0.088	0.297	26.9
Mintsa et al [35]	20.1	0.1	0.323	31.4
Ho et al. [79]	19.2	0.095	0.308	28.4
RSM	3.7	0.007	0.0841	14.3

Table 11. The mathematical expressions of statistical parameters used in this study.

Statistical parameters	Formula
Average absolute relative deviation percent (AARD%) [80]	$AARD\% = \frac{100}{n} \sum_i \frac{ P_{iexp} - P_{ipred} }{P_{iexp}}$
MSE [80]	$MSE = \frac{1}{n} \sum_i (P_{iexp} - P_{ipred})^2$
Root Mean Square Error (RMSE) [76]	$RMSE = \sqrt{\frac{1}{n} \sum_i (P_{iexp} - P_{ipred})^2}$
Margin of deviation (MOD%) [81]	$MOD\% = \frac{P_{ipred} - P_{iexp}}{P_{iexp}} \times 100$

6. Conclusion

In this study, thermal conductivity of Al₂O₃/water nanofluid was investigated. RSM was effectively utilized in this study, yielding equations that accurately estimate the KR of the nanofluid. RSM provided different equations to calculate KR based on independent parameters such as SVF and T. The quadratic model has been demonstrated to be superior to the other models through the use of statistical parameters and plots. R², adjusted R², predicted R² and Std. Dev parameters of the quadratic model were equal to 0.9785, 0.9606, 0.8776 and 0.0241 respectively, which signifies the accuracy of the model. As well, the difference between adjusted R² and predicted R² is less than 0.083 indicates the high accuracy of the proposed model. The residual plot, the normal probability plot, the Box-Cox plot and the predicted vs. actual plot also showed that quadratic model has a good accuracy, and is well capable of estimating the KR of the nanofluid. The experimental outcomes displayed that a raise in SVF and T caused an increase in KR. This trend was estimated by RSM methods with very high accuracy. Ultimately, the optimum combination for better KR was found at SVF = 1.764% and T = 45 °C.

Nomenclature

2FI	two-factor interaction
AAD	average absolute deviation
ANOVA	analysis of variance
C.D	correlation deviation
CV (%)	coefficient of Variation
D	dimention
DF	degrees of Freedom
DLS	dynamic light scattering
EG	ethylene glycol
GNP	graphene nanoplatelets
GO	graphene oxide
h	hour
HNF	hybrid nanofluid
KR	Thermal conductivity ration (Knf/Kbf)
MOD	margin of deviation
MSE	mean square error
MWCNT	multi-walled carbon nanotubes
ND	nanodiamond
R ²	coefficient of determination(-)
RSM	response surface methodology
SR	Shear rate
Std. Dev	standard deviation
SVF	solid volume fraction
T	Temperature (°C)
TEM	Transmission electron microscopy
VIF	variance Inflation Factors
vol	volume
W	water

Greek symbols

λ	lambda value
-----------	--------------

Subscripts

bf	base fluid
Exp	experimental
Pred	predicted

Accepted Manuscript

References

1. Choi, S.U.S. *Enhancing thermal conductivity of fluids with nanoparticles*. in *Proceedings of the 1995 ASME International Mechanical Engineering Congress and Exposition*. 1995. New York, USA.
2. Wang, X.-j., D.-s. Zhu, and S. yang, *Investigation of pH and SDBS on enhancement of thermal conductivity in nanofluids*. *Chemical Physics Letters*, 2009. **470**(1–3): p. 107-111.
3. Zhu, D., et al., *Dispersion behavior and thermal conductivity characteristics of Al₂O₃-H₂O nanofluids*. *Current Applied Physics*, 2009. **9**(1): p. 131-139.
4. Shahsavari, A., et al., *Impact of variable fluid properties on forced convection of Fe₃O₄/CNT/water hybrid nanofluid in a double-pipe mini-channel heat exchanger*. *Journal of Thermal Analysis and Calorimetry*, 2019. **137**: p. 1031-1043.
5. Kumar, N., et al., *Experimental study on pool boiling and Critical Heat Flux enhancement of metal oxides based nanofluid*. *International Communications in Heat and Mass Transfer*, 2018. **96**: p. 37-42.
6. Vijay, J. and S. Sonawane Shriram, *Investigations on rheological behaviour of paraffin based Fe₃O₄ nanofluids and its modelling*. *Res. J. Chem. Environ*, 2015. **19**(12): p. 22-29.
7. Kumar, N., S.S. Sonawane, and S.H. Sonawane, *Experimental study of thermal conductivity, heat transfer and friction factor of Al₂O₃ based nanofluid*. *International Communications in Heat and Mass Transfer*, 2018. **90**: p. 1-10.
8. Bhanvase, B.A., et al., *Intensified heat transfer rate with the use of nanofluids*, in *Handbook of nanomaterials for industrial applications*. 2018, Elsevier. p. 739-750.
9. Malika, M.M. and S.S. Sonawane, *Review on application of nanofluid/nano particle as water disinfectant*. *Journal of Indian Association for Environmental Management (JIAEM)*, 2019. **39**(1-4): p. 21-24.
10. Khan, M., et al., *Investigation of thermal and mechanical properties of styrene-butadiene rubber nanocomposites filled with SiO₂-polystyrene core-shell nanoparticles*. *Journal of Composite Materials*, 2020. **54**(14): p. 1785-1795.
11. Yu, W. and S. Choi, *The role of interfacial layers in the enhanced thermal conductivity of nanofluids: a renovated Maxwell model*. *Journal of nanoparticle research*, 2003. **5**(1-2): p. 167-171.
12. Nadooshan, A.A., *An experimental correlation approach for predicting thermal conductivity of water-EG based nanofluids of zinc oxide*. *Physica E: Low-dimensional Systems and Nanostructures*, 2017. **87**: p. 15-19.
13. Esfe, M.H., et al., *Optimization, modeling and accurate prediction of thermal conductivity and dynamic viscosity of stabilized ethylene glycol and water mixture Al₂O₃ nanofluids by NSGA-II using ANN*. *International Communications in Heat and Mass Transfer*, 2017. **82**: p. 154-160.
14. Esfe, M.H., et al., *Experimental evaluation, sensitivity analysis and ANN modeling of thermal conductivity of ZnO-MWCNT/EG-water hybrid nanofluid for engineering applications*. *Applied Thermal Engineering*, 2017. **125**: p. 673-685.
15. Esfe, M.H., *Designing a neural network for predicting the heat transfer and pressure drop characteristics of Ag/water nanofluids in a heat exchanger*. *Applied Thermal Engineering*, 2017. **126**: p. 559-565.
16. Heris, S.Z., et al., *A comparative experimental study on the natural convection heat transfer of different metal oxide nanopowders suspended in turbine oil inside an inclined cavity*. *International Journal of Heat and Mass Transfer*, 2014. **73**: p. 231-238.
17. Mahian, O., et al., *Natural convection of silica nanofluids in square and triangular enclosures: theoretical and experimental study*. *International Journal of Heat and Mass Transfer*, 2016. **99**: p. 792-804.
18. Afrand, M., *Experimental study on thermal conductivity of ethylene glycol containing hybrid nano-additives and development of a new correlation*. *Applied Thermal Engineering*, 2017. **110**: p. 1111-1119.

19. Afrand, M., K.N. Najafabadi, and M. Akbari, *Effects of temperature and solid volume fraction on viscosity of SiO₂-MWCNTs/SAE40 hybrid nanofluid as a coolant and lubricant in heat engines*. Applied Thermal Engineering, 2016. **102**: p. 45-54.
20. Afrand, M., D. Toghraie, and N. Sina, *Experimental study on thermal conductivity of water-based Fe₃O₄ nanofluid: development of a new correlation and modeled by artificial neural network*. International Communications in Heat and Mass Transfer, 2016. **75**: p. 262-269.
21. Esfe, M.H., et al., *Thermal conductivity enhancement of SiO₂-MWCNT (85: 15%)-EG hybrid nanofluids*. J Therm Anal Calorim, 2017. **128**(1): p. 249-258.
22. Esfe, M.H. and M.H. Hajmohammad, *Thermal conductivity and viscosity optimization of nanodiamond-Co₃O₄/EG (40: 60) aqueous nanofluid using NSGA-II coupled with RSM*. Journal of Molecular Liquids, 2017. **238**: p. 545-552.
23. Esfe, M.H., et al., *Designing an artificial neural network to predict dynamic viscosity of aqueous nanofluid of TiO₂ using experimental data*. International communications in heat and mass transfer, 2016. **75**: p. 192-196.
24. Esfe, M.H., et al., *The optimization of viscosity and thermal conductivity in hybrid nanofluids prepared with magnetic nanocomposite of nanodiamond cobalt-oxide (ND-Co₃O₄) using NSGA-II and RSM*. International Communications in Heat and Mass Transfer, 2016. **79**: p. 128-134.
25. Rostamian, S.H., et al., *An inspection of thermal conductivity of CuO-SWCNTs hybrid nanofluid versus temperature and concentration using experimental data, ANN modeling and new correlation*. Journal of Molecular Liquids, 2017. **231**: p. 364-369.
26. Zhang, Y.-Y., et al., *Thermal conductivity of penta-graphene: the role of chemical functionalization*. Computational Materials Science, 2017. **137**: p. 195-200.
27. Esfe, M.H., et al., *Estimation of thermal conductivity of Al₂O₃/water (40%)-ethylene glycol (60%) by artificial neural network and correlation using experimental data*. International Communications in Heat and Mass Transfer, 2016. **74**: p. 125-128.
28. Bashirnezhad, K., et al., *Viscosity of nanofluids: a review of recent experimental studies*. International Communications in Heat and Mass Transfer, 2016. **73**: p. 114-123.
29. Hemmat Esfe, M., et al., *Thermal conductivity of Al₂O₃/water nanofluids: measurement, correlation, sensitivity analysis, and comparisons with literature reports*. Journal of Thermal Analysis and Calorimetry, 2014. **117**: p. 675-681.
30. Putra, N., W. Roetzel, and S.K. Das, *Natural convection of nano-fluids*. Heat and mass transfer, 2003. **39**(8): p. 775-784.
31. Zhang, X., H. Gu, and M. Fujii, *Experimental study on the effective thermal conductivity and thermal diffusivity of nanofluids*. International Journal of Thermophysics, 2006. **27**: p. 569-580.
32. Masuda, H., A. Ebata, and K. Teramae, *Alteration of thermal conductivity and viscosity of liquid by dispersing ultra-fine particles. Dispersion of Al₂O₃, SiO₂ and TiO₂ ultra-fine particles*. 1993.
33. Eastman, J.A., et al., *Anomalously increased effective thermal conductivities of ethylene glycol-based nanofluids containing copper nanoparticles*. Applied physics letters, 2001. **78**(6): p. 718-720.
34. Murshed, S., K. Leong, and C. Yang, *Enhanced thermal conductivity of TiO₂-water based nanofluids*. International Journal of thermal sciences, 2005. **44**(4): p. 367-373.
35. Mintsu, H.A., et al., *New temperature dependent thermal conductivity data for water-based nanofluids*. International journal of thermal sciences, 2009. **48**(2): p. 363-371.
36. Abdel-Samad, S.M., et al., *Experimental investigation of TiO₂-water nanofluids thermal conductivity synthesized by Sol-gel technique*. Current Nanoscience, 2017. **13**(6): p. 586-594.
37. Eshgarf, H., et al., *Experimental examination of the properties of Fe₃O₄/water nanofluid, and an estimation of a correlation using an artificial neural network*. Journal of Molecular Liquids, 2023: p. 121150.
38. Jahan, A., K.L. Edwards, and M. Bahraminasab, *6 - Multiple objective decision-making for material and geometry design*, in *Multi-criteria Decision Analysis for Supporting the Selection of Engineering Materials in Product Design (Second Edition)*, A. Jahan, K.L. Edwards, and M. Bahraminasab, Editors. 2016, Butterworth-Heinemann. p. 127-146.

39. Malika, M. and S.S. Sonawane, *Application of RSM and ANN for the prediction and optimization of thermal conductivity ratio of water based Fe₂O₃ coated SiC hybrid nanofluid*. International Communications in Heat and Mass Transfer, 2021. **126**: p. 105354.
40. Esfe, M.H., M. Firouzi, and M. Afrand, *Experimental and theoretical investigation of thermal conductivity of ethylene glycol containing functionalized single walled carbon nanotubes*. Physica E: Low-dimensional Systems and Nanostructures, 2018. **95**: p. 71-77.
41. Peng, Y., et al., *Potential application of Response Surface Methodology (RSM) for the prediction and optimization of thermal conductivity of aqueous CuO (II) nanofluid: A statistical approach and experimental validation*. Physica A: Statistical Mechanics and its Applications, 2020. **554**: p. 124353.
42. Esfe, M.H., et al., *The effect of different parameters on ability of the proposed correlations for the rheological behavior of SiO₂-MWCNT (90: 10)/SAE40 oil-based hybrid nano-lubricant and presenting five new correlations*. ISA transactions, 2022. **128**: p. 488-497.
43. Khetib, Y., et al., *Competition of ANN and RSM techniques in predicting the behavior of the CuO-liquid paraffin*. Chemical Engineering Communications, 2023. **210**(6): p. 880-892.
44. Esfe, M.H., et al., *Prediction and optimization of thermophysical properties of stabilized Al₂O₃/antifreeze nanofluids using response surface methodology*. Journal of Molecular Liquids, 2018. **261**: p. 14-20.
45. Khetib, Y., et al., *Using neural network and RSM to evaluate improvement in thermal conductivity of nanodiamond-iron oxide/antifreeze*. Chemical Engineering Communications, 2023. **210**(4): p. 596-606.
46. Khetib, Y., K. Sedraoui, and A. Gari, *Improving thermal conductivity of a ferrofluid-based nanofluid using Fe₃O₄-challenging of RSM and ANN methodologies*. Chemical Engineering Communications, 2022. **209**(8): p. 1070-1081.
47. Shahsavar, A., et al., *Thermal conductivity of hydraulic oil-GO/Fe₃O₄/TiO₂ ternary hybrid nanofluid: experimental study, RSM analysis, and development of optimized GPR model*. Journal of Molecular Liquids, 2023. **385**: p. 122338.
48. Borode, A. and P. Olubambi, *Modelling the effects of mixing ratio and temperature on the thermal conductivity of GNP-Alumina hybrid nanofluids: A comparison of ANN, RSM, and linear regression methods*. Heliyon, 2023. **9**(8).
49. Esfe, M.H., et al., *Measurement of thermal conductivity of triple hybrid water based nanofluid containing MWCNT (10%)-Al₂O₃ (60%)-ZnO (30%) nanoparticles*. Colloids and Surfaces A: Physicochemical and Engineering Aspects, 2022. **647**: p. 129083.
50. Esfe, M.H., et al., *Thermal conductivity of MWCNT-TiO₂/Water-EG hybrid nanofluids: Calculating the price performance factor (PPF) using statistical and experimental methods (RSM)*. Case Studies in Thermal Engineering, 2023. **48**: p. 103094.
51. Mukherjee, S., P.C. Mishra, and P. Chaudhuri, *Stability of heat transfer nanofluids—a review*. ChemBioEng Reviews, 2018. **5**(5): p. 312-333.
52. Raei, B., et al., *Experimental study on the heat transfer and flow properties of γ -Al₂O₃/water nanofluid in a double-tube heat exchanger*. Journal of Thermal Analysis and Calorimetry, 2017. **127**(3): p. 2561-2575.
53. Raei, B., et al., *Experimental investigation on the heat transfer performance and pressure drop characteristics of γ -Al₂O₃/water nanofluid in a double tube counter flow heat exchanger*. Challenges in Nano and Micro Scale Science and Technology, 2016. **5**(1): p. 64-75.
54. Raei, B., *Statistical analysis of nanofluid heat transfer in a heat exchanger using Taguchi method*. Journal of Heat and Mass Transfer Research, 2021. **8**(1): p. 29-38.
55. Raei, B., S. Peyghambarzadeh, and R.S. Asl, *Experimental investigation on heat transfer and flow resistance of drag-reducing alumina nanofluid in a fin-and-tube heat exchanger*. Applied Thermal Engineering, 2018. **144**: p. 926-936.
56. Raei, B. and S.M. Peyghambarzadeh, *Measurement of Local Convective Heat Transfer Coefficient of Alumina-Water Nanofluids in a Double Tube Heat Exchanger*. Journal of Chemical and Petroleum engineering, 2019. **53**(1): p. 25-36.
57. Mukherjee, S., et al., *Enhancing thermophysical characteristics and heat transfer potential of TiO₂/water nanofluid*. International Journal of Thermophysics, 2020. **41**(12): p. 1-33.

58. Ali, N., J.A. Teixeira, and A. Addali, *A review on nanofluids: fabrication, stability, and thermophysical properties*. Journal of Nanomaterials, 2018. **2018**.
59. Cabaleiro, D., et al., *Heat transfer capability of (ethylene glycol+ water)-based nanofluids containing graphene nanoplatelets: Design and thermophysical profile*. Nanoscale research letters, 2017. **12**(1): p. 1-11.
60. Fedele, L., et al., *Experimental stability analysis of different water-based nanofluids*. Nanoscale research letters, 2011. **6**: p. 1-8.
61. Teng, T.-P., et al., *The effect of alumina/water nanofluid particle size on thermal conductivity*. Applied Thermal Engineering, 2010. **30**(14-15): p. 2213-2218.
62. Sodeifian, G., J. Azizi, and S. Ghoreishi, *Response surface optimization of Smyrniun cordifolium Boiss (SCB) oil extraction via supercritical carbon dioxide*. The Journal of Supercritical Fluids, 2014. **95**: p. 1-7.
63. Sodeifian, G., N. Saadati Ardestani, and S.A. Sajadian, *Extraction of seed oil from Diospyros lotus optimized using response surface methodology*. Journal of Forestry Research, 2019. **30**(2): p. 709-719.
64. Sodeifian, G., et al., *Properties of Portulaca oleracea seed oil via supercritical fluid extraction: Experimental and optimization*. The Journal of Supercritical Fluids, 2018. **135**: p. 34-44.
65. Sodeifian, G., S.A. Sajadian, and B. Honarvar, *Mathematical modelling for extraction of oil from Dracocephalum kotschy seeds in supercritical carbon dioxide*. Natural Product Research, 2018. **32**(7): p. 795-803.
66. Sodeifian, G., S.A. Sajadian, and N.S. Ardestani, *Experimental optimization and mathematical modeling of the supercritical fluid extraction of essential oil from Eryngium billardieri: Application of simulated annealing (SA) algorithm*. The journal of supercritical fluids, 2017. **127**: p. 146-157.
67. Ameri, A., G. Sodeifian, and S.A. Sajadian, *Lansoprazole loading of polymers by supercritical carbon dioxide impregnation: Impacts of process parameters*. The Journal of Supercritical Fluids, 2020. **164**: p. 104892.
68. Fathi, M., G. Sodeifian, and S.A. Sajadian, *Experimental study of ketoconazole impregnation into polyvinyl pyrrolidone and hydroxyl propyl methyl cellulose using supercritical carbon dioxide: Process optimization*. The Journal of Supercritical Fluids, 2022. **188**: p. 105674.
69. Ardestani, N.S., G. Sodeifian, and S.A. Sajadian, *Preparation of phthalocyanine green nano pigment using supercritical CO2 gas antisolvent (GAS): experimental and modeling*. Heliyon, 2020. **6**(9).
70. Sodeifian, G., S.A. Sajadian, and R. Derakhsheshpour, *CO2 utilization as a supercritical solvent and supercritical antisolvent in production of sertraline hydrochloride nanoparticles*. Journal of CO2 Utilization, 2022. **55**: p. 101799.
71. Hazaveie, S.M., G. Sodeifian, and N.S. Ardestani, *Micro and nanosizing of Tamsulosin drug via supercritical CO2 antisolvent (SAS) process*. Journal of CO2 Utilization, 2024. **84**: p. 102847.
72. Lau, H.-L., et al., *Optimization of fermentation medium components by response surface methodology (RSM) and artificial neural network hybrid with genetic algorithm (ANN-GA) for lipase production by Burkholderia cenocepacia ST8 using used automotive engine oil as substrate*. Biocatalysis and Agricultural Biotechnology, 2023. **50**: p. 102696.
73. Hussain, S., et al., *Modeling of photolytic degradation of sulfamethoxazole using boosted regression tree (BRT), artificial neural network (ANN) and response surface methodology (RSM); energy consumption and intermediates study*. Chemosphere, 2021. **276**: p. 130151.
74. Borode, A.O., et al., *Effect of various surfactants on the viscosity, thermal and electrical conductivity of graphene nanoplatelets nanofluid*. International Journal of Thermophysics, 2021. **42**(11): p. 158.
75. Amiri, A., M. Shanbedi, and H. Dashti, *Thermophysical and rheological properties of water-based graphene quantum dots nanofluids*. Journal of the Taiwan Institute of Chemical Engineers, 2017. **76**: p. 132-140.
76. Rostamian, H. and M.N. Lotfollahi, *A novel statistical approach for prediction of thermal conductivity of CO2 by Response Surface Methodology*. Physica A: Statistical Mechanics and its Applications, 2019. **527**: p. 121175.
77. Wasp, E.J., J.P. Kenny, and R.L. Gandhi, *Solid-liquid flow: slurry pipeline transportation.[Pumps, valves, mechanical equipment, economics]*. Ser. Bulk Mater. Handl.:(United States), 1977. **1**(4).

78. Williams, W., J. Buongiorno, and L.-W. Hu, *Experimental investigation of turbulent convective heat transfer and pressure loss of alumina/water and zirconia/water nanoparticle colloids (nanofluids) in horizontal tubes*. Journal of Heat Transfer, 2008. **130**(4): p. 042412.
79. Ho, C., et al., *Natural convection heat transfer of alumina-water nanofluid in vertical square enclosures: an experimental study*. International Journal of Thermal Sciences, 2010. **49**(8): p. 1345-1353.
80. Rostamian, H. and M.N. Lotfollahi, *A new simple equation of state for calculating solubility of solids in supercritical carbon dioxide*. Periodica Polytechnica Chemical Engineering, 2015. **59**(3): p. 174-185.
81. Zha, T.-H., et al., *A fuzzy-based strategy to suppress the novel coronavirus (2019-NCOV) massive outbreak*. Applied and Computational Mathematics, 2021: p. 160-176.

Accepted Manuscript